CrystEngComm

Accepted Manuscript

ROYAL SOCIETY OF CHEMISTRY

www.rsc.org/crystengcomm

Journal Name

RSCPublishing

COMMUNICATION

Fabrication of coupled twin-shaped hollow hemispherical calcium molybdate via a facile ultrasound-assisted approach

Cite this: DOI: 10.1039/x0xx00000x

Yongfang Zhang,[a,c] Limin Wang,*[,b,c] Deqing Chu,*[,a] Hongming Sun,[a] Aoxuan Wang,[a] Zhongchao Ma,[b] Lufeng Yang,[a] Yan Zhuang[a] and Yuze Bai[a]

Received 00th January 2012,
Accepted 00th January 2012

DOI: 10.1039/x0xx00000x

www.rsc.org/

Coupled twin-shaped hollow hemispherical calcium molybdate （CTHH-$CaMoO_4$）microstructure was successfully synthesized via a facile ultrasound-assisted template-free route in the presence of absolute ethanol and ethylenediamine tetraacetic acid (EDTA). The oriented attachment and subsequent Ostwald ripening mechanism were responsible for the formation of this novel architecture.

It is well-known that properties of materials can be profoundly affected by their morphologies, and the structure-function relationship is the underlying motive for discovering and fabricating novel structures. Recently, tremendous scientific efforts have been devoted to the inorganic hollow micro/nanostructures[1-3] owing to their higher specific surface area, lower density, better permeability, and more widespread applications in many fields compared with their entity counterparts. $CaMoO_4$, as an important member of the metal molybdate families, has promising applications in various fields, such as electro-optical devices,[4] scintillators,[5] photoluminescence[6-8] and so forth. Up to now, different morphologies of $CaMoO_4$, including nanoparticles,[9] nanorods,[10,11] microclews,[12] notched microspheres,[13] flower-like structures,[14,15] persimmon-like micro/nanomaterials[16] and erythrocyte-like hierarchical nanostructures[17] have been successfully fabricated by microemulsion method,[14] hydrothermal reaction,[6,12] template-based rheological phase reaction route[11] and so on. However, to the best of our knowledge, there are rare reports about the fabrication of hollow $CaMoO_4$ architectures.[18] Therefore, hollow $CaMoO_4$ microstructures, reducing material consumption and enhancing performance are urgent to be developed.

The sonochemical process has been proven to be an effective technique to obtain novel materials with unique morphologies and properties.[19-21] In contrast with other synthesis methods, the sonochemical method is advantageous as it is nonhazardous, clean, facile and rapid in reaction rate. So far, the sonochemical method has been used to prepare numerous hollow materials, including PbS,[22] CdSe,[23] MoS_2,[24] etc. As to mechanism, various known physical phenomena, such as oriented attachment,[25] corrosion-based inside-out evacuation,[26] Kirkendall effect,[27] and Ostwald ripening[28] have been employed in template-free fabrications of inorganic hollow structures. Thereinto, Ostwald ripening is a near-equilibrium process of aging, redistribution, or coarsening of matter, in which smaller, or less dense particles in an aggregate dissolve gradually, while larger, or denser particles in the same aggregate are growing to minimize surface energy.[29]

In this paper, we took an environmentally friendly ultrasound-assisted template-free approach at room temperature to synthesize well-defined CTHH-$CaMoO_4$ architecture. Compared with the reactions in pure water, synthesis of micro/nanomaterials in an ethanol-water mixture was favorable for the solvent properties changed.[30,31] EDTA, as the structure-directing agent,[32,33] also makes a significant contribution to this unique CTHH-$CaMoO_4$ morphology. Time-dependent experiments were conducted to observe the morphology evolution. Based on the experimental results, a possible hollow structure formation mechanism related to Ostwald ripening process was proposed.

All chemicals were of analytical grade and used without further purification. In a typical procedure, 1 mmol calcium chloride ($CaCl_2$) and 0.02 mmol EDTA were added into 20 mL of mixed solvent （The volume ratio of ethanol to deionized water R = 1:1）to form solution A, which was stirred at room temperature for 30 min to be fully homogenized. Then 0.6 mmol sodium molybdate （Na_2MoO_4） was added into another 20 mL mixed solvent with the same ratio to form solution B. Next, solution B was rapidly mixed with solution A to form a turbid liquid, which was disposed under continuous magnetic agitation for another 15 min. After that, the resulting turbid liquid was treated by ultrasound irradiation at ambient atmosphere for 30 min by an ordinary ultrasound cleaning bath. Finally, the obtained products were collected by centrifugation, washed several times with deionized water and ethanol, and dried in vacuum at 60 ℃ for 12 h.

Fig. 1 presents scanning electron microscopy (SEM) and X-ray diffraction (XRD) images of the as-prepared uniform CTHH-$CaMoO_4$. A panoramic morphology of the product is displayed in Fig. 1a,

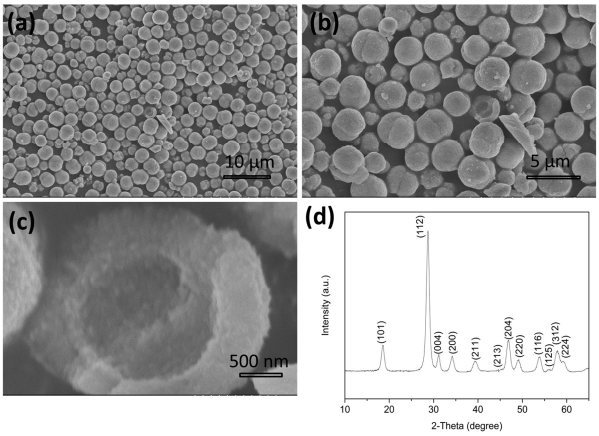

Fig. 1 SEM images and XRD pattern of the as-synthesized CTHH-$CaMoO_4$: (a) Overall product morphology; (b) a magnified SEM image; (c) a close-up image of an individual CTHH-$CaMoO_4$; (d) a representative XRD pattern recorded for the CTHH-$CaMoO_4$.

indicating that a large scale of coupled hemispheres are achieved. A magnified SEM image showing the closer observation of the microstructure is given in Fig. 1b, which reveals that the detailed morphology of $CaMoO_4$ product is well-defined coupled twin-shaped hollow hemisphere with diameters in the range of 2–3 μm. Fig. 1c shows an individual broken coupled hemisphere, and it can be seen that the interior is hollow and the thickness of the shell is ~400 nm. The phase of the synthesized $CaMoO_4$ microcrystals was identified by XRD characterization. As shown in Fig. 1d, all the diffraction peaks can be indexed to tetragonal $CaMoO_4$ (JCPDS-ICDD card No. 7–212).[16] No peaks of impurity are detected in the XRD pattern, indicating the formation of pure $CaMoO_4$ under these experimental conditions.

The volume ratio of ethanol to deionized water (R=v/v) in the reaction solution is an important factor in determining the structure and morphology of the final $CaMoO_4$ samples. In the absence of ethanol, flowerlike spheres (Fig. 2a) assembled by nanoplates were obtained. When the volume ratio was R = 1/9, messy spheres with trace amount of flowerlike spheres (Fig. 2b) were generated. As the volume ratio increased to R = 1/3, aggregated microspheres with the diameter of about 1.5 μm (Fig. 2c) were achieved. It can be seen from Fig. 2d that irregular nanorods assembled together unorientedly with the volume ratio R = 3.

It is well known that solvent properties greatly influence the solubility and transport behaviour of the reactant, and will further influence the morphology of the product. With the increase of ethanol in the mixed solvent, the polarity of the solution decreases and the solubility of the reactant decreases similarly.[30] In addition, the H_2O molecule is small enough to be easily polarized, which can effectively stabilize the ions in the solution, leading to the low reactivity of the reactant.[31] It has been reported that the decreased solvent polarity causes decreased tendency of oriented attachment of the primary nanoparticles.[34] Fig. 2a shows that without ethanol, the polarity of the solvent is relatively high, which gives the primary particles enough time to assemble into regular nanoplates and the nanoplates assemble further into flowerlike spheres. With the increased fraction of ethanol, the reactivity of the ions in the solution increases, so the number of

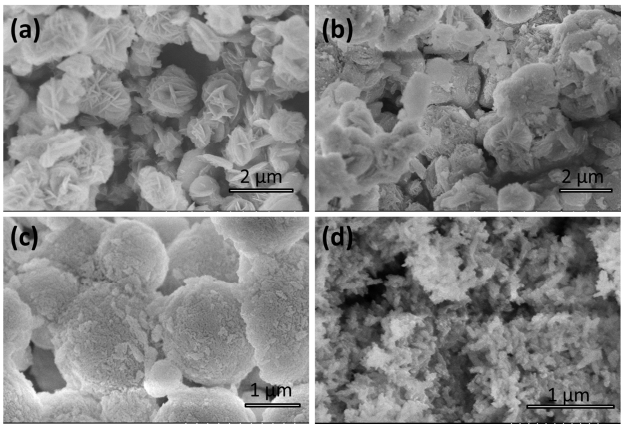

Fig. 2 SEM images of the $CaMoO_4$ samples produced with different volume ratio of ethanol to deionized water (R=v/v): (a) R = 0; (b) R = 1/9; (c) R = 1/3; (d) R = 3.

nucleation particles is larger and the reaction rate is faster, which results in little time to age and aggregate the particles in order and to generate the product with irregular morphologies.[31] In our experiments, different morphologies of $CaMoO_4$ products such as messy spheres in Fig. 2b, aggregated microspheres in Fig. 2c, and finally irregular assembled nanorods in Fig. 2d were obtained with increasing the amount of ethanol.

The presence of an appropriate amount of EDTA plays vital structure-directing role in the formation of this unique CTHH-$CaMoO_4$ architecture. It is obvious that with the addition of EDTA increasing, the split degree of the crystals increases (Fig. 3).[35,36] Controlled experiments showed that without the addition of EDTA in the reaction system, peony-shaped hierarchical architecture assembled by nanorods was obtained, as shown in Fig. 3a and b. As the amount of EDTA is

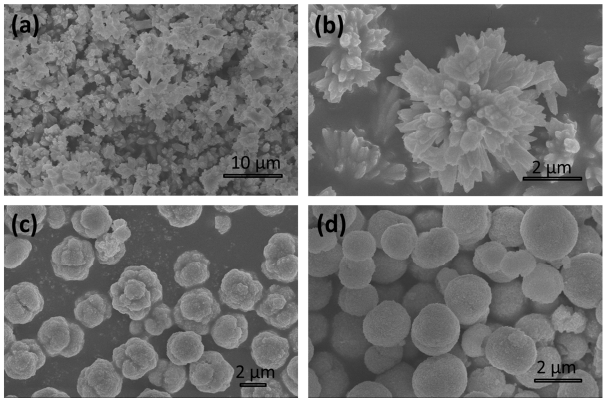

Fig. 3 SEM images of the obtained samples in the presence of different amount of EDTA: (a) and (b) 0 mmol, (c) 0.01 mmol, and (d) 0.04 mmol.

0.01mmol, the outline of the product was coupled twin-shaped as well as cauliflower-shaped hemispheres with rugged surface (Fig. 3c), and the overall dispersity and uniformity are poor. If the amount of EDTA increases to 0.04 mmol, the split degree increases further, and most of the obtained particles were single microspheres (Fig. 3d) instead of

uniform coupled hemispheres (Fig. 1b). It can be concluded from the above phenomena that EDTA acted as an efficient crystal-growth modifier to modify the morphology of the product.[33]

For a substantial view of the growth mechanism of the CTHH-$CaMoO_4$ architecture, time-dependent evolution process was monitored. The samples obtained at various reaction times were inspected by SEM and TEM. The temporal evolution of the resulting structure is shown in Fig. 4. Obviously, the primary particles in the range of 20–30 nm （Fig. 4a, b） formed once solution B was mixed with solution A. After continuous magnetic agitation for 15 min, the coupled twin-shaped hemispherical entity $CaMoO_4$ microstructures were obtained (Fig. 4c, d), as we can observe from a broken coupled twin-shaped hemisphere. If ultrasonic treatment was further implemented to the above product for 10 min, partial hollow coupled twin-shaped hemispheres were achieved (Fig. 4e, f), the thickness of the shell varies from 200 nm to 400 nm. As shown in Fig. 1b and c, completely hollow coupled hemispheres were generated with prolonging the ultrasonic time to 30 min, while the outline and average particle size changed little. Interestingly, hollow interior can't be obtained without ultrasonic processing even aging for a relatively long time (1 hour, 10 hours and 1 day). Regarding the synthesis of hollow interiors, it is recognized that the ripening process involves the mass transfer between the solid core and outside chemical solution under ultrasonic treatment.[28]

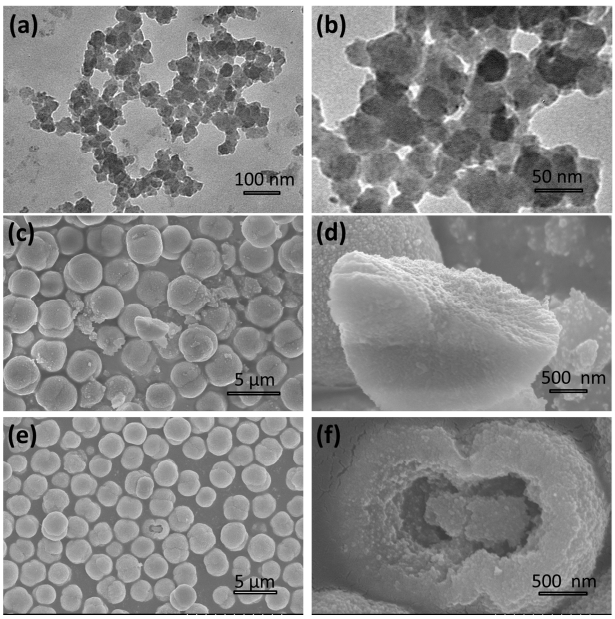

Fig. 4 TEM and SEM images of products obtained at various reaction times: (a) and (b) 0 min; (c) and (d) 15 min (continuous magnetic agitation); (e) and (f) 25 min (including 15 min continuous magnetic agitation and 10 min ultrasonic treatment).

In order to verify the crystal form of the time-dependent products, XRD patterns were presented in Fig. 5. It can be seen that the crystallinity was considerably low when the reaction time was 0 min (Fig. 5a), and increased gradually with the reaction time prolonged (Fig. 5b, c), especially when ultrasound was implemented. When the reaction time was 45 min, well-crystallized CTHH-$CaMoO_4$ were obtained (Fig. 5d), while the location of the peaks and crystal form remained throughout the whole process.

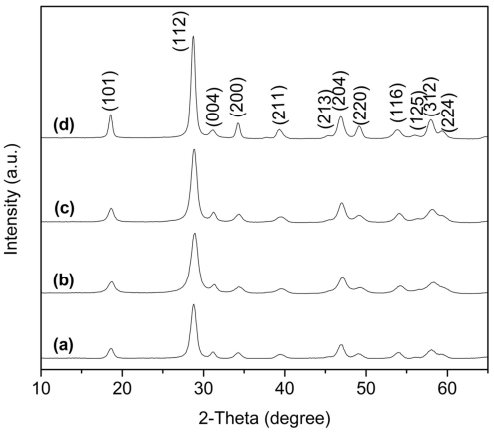

Fig. 5 Time-dependent XRD patterns: (a) 0 min; (b) 15 min (continuous magnetic agitation); (c) 25 min (including 15 min continuous magnetic agitation and 10 min ultrasonic treatment); (d) 45 min (including 15 min continuous magnetic agitation and 30 min ultrasonic treatment).

The growth pathway of $CaMoO_4$ microstructures from primary particles to coupled twin-shaped hemispherical entities was investigated at various intervals by TEM/HR-TEM. Fig. 6a illustrates the low magnification TEM micrograph of shuttle-like $CaMoO_4$ oriented aggregate crystals obtained when the reaction time was 1 min. HR-TEM performed in the corner of the shuttle-like morphology (dashed white square in Fig. 6a) reveals that the lattice fringes were a little obscure (Fig. 6b). As the reaction time prolonged to 5 min, shuttle-like $CaMoO_4$ transformed to straw-like structures (Fig. 6c) through imperfect oriented attachment,[37] as can be confirmed by the dislocations of the lattice fringes in Fig. 6d. The lattice fringes spaced at *ca.* 3.12 Å, which correspond to the distance of the (112) plane of tetragonal $CaMoO_4$, become clear. The crystals maturated at 15 min exhibited coupled twin-shaped hemispherical morphology (Fig. 6e). In this sample, the 3.12 Å lattice fringes were more clearly and frequently observed than at 5 min, confirming the increased crystallinity and the ordered structure of these nanoparticles (Fig. 6f),[38] which has been demonstrated by the XRD patterns in Fig. 5. Further observation to it, the spontaneous self-organization of adjacent particles can be seen, they would rotate and have contact with each other until the crystallographic orientation of the two crystals match (black arrow marked with oriented attachment).[39] Then they share a common crystallographic orientation, followed by joining of these particles at a planar interface to reduce the overall surface energy, which is in agreement with previous results.[37] The values of the length and width of the crystals at various intervals were observed (see the ESI Fig. S1). It can be seen from Fig. S1a and b that most of shuttle-like $CaMoO_4$ microstructures were in the range of 200–400 nm in length and 100–200 nm in width at 1 min. Fig. S1c and d demonstrated straw-like morphologies about 600 nm–800 nm in length and 300–400 nm in width obtained at 5 min. Coupled twin-shaped hemispherical microstructures about 3–4 μm in length and 2–3 μm in width were generated at 15 min (Fig. S1e and f). The gradual

increase of length and width of the crystals can further identify the existence of oriented attachment process.

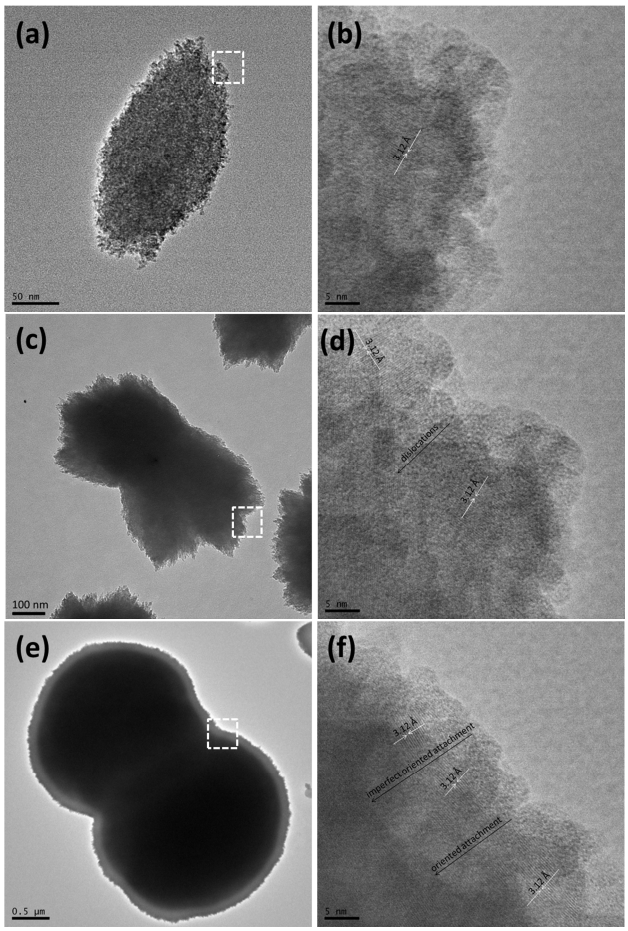

Fig. 6 TEM and HR-TEM micrographs of the samples at various intervals: (a) and (b) 1 min; (c) and (d) 5 min; (e) and (f) 15 min. (b, d and f are corresponding HR-TEM images performed on the edge of the crystal from a, c and e, respectively. The lattice fringes spaced at *ca.* 3.12 Å correspond to the distance of the (112) plane of tetragonal $CaMoO_4$.)

On the basis of above analysis, it is reasonable to speculate that the formation of CTHH-$CaMoO_4$ structure is based on the oriented attachment and subsequent Ostwald ripening mechanism,[28,40,41] and the evolution process is illustrated in Fig. 7. In this process, primary

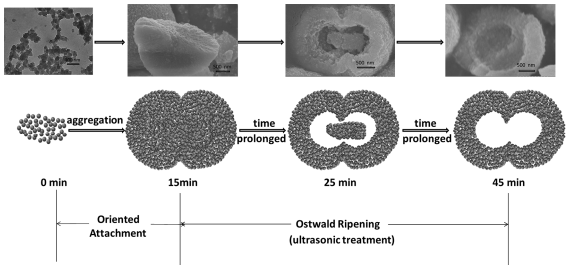

Fig. 7 Schematic formation process based on the oriented attachment and Ostwald ripening mechanism.

$CaMoO_4$ nuclei aggregate into solid coupled twin-shaped hemispheres through oriented attachment in the solution to minimize the surface energy. The positive influence of ultrasonic treatment caused local hotspots and cavitation effects,[21] a phenomenon occurring when a liquid is exposed to high power ultrasound. And the creation of these extreme conditions can drive a variety of chemical reactions, such as dissolution. Then redistribution happens with the assistance of ultrasonic treatment, larger crystallites outside are essentially immobile while the unstable smaller ones inside are undergoing mass relocation through dissolving and regrowing, which creates the interior space within the original aggregates. Finally, solid cores are consumed and disappear, forming the hollow cavity inside the coupled hemisphere.

The nitrogen adsorption-desorption isotherms of coupled twin-shaped hemispherical $CaMoO_4$ before and after the ultrasonic treatment are shown in Fig. 8. As can be seen, both isotherms exhibit stepwise adsorption and desorption, which indicate the presence of mesoporosity in the samples.[42,43] The Brunauer-Emmett-Teller (BET) surface areas for them are 125.2 and 142.4 $m^2 \cdot g^{-1}$, respectively. The larger BET surface area of the latter one may come from the hollow interior, which

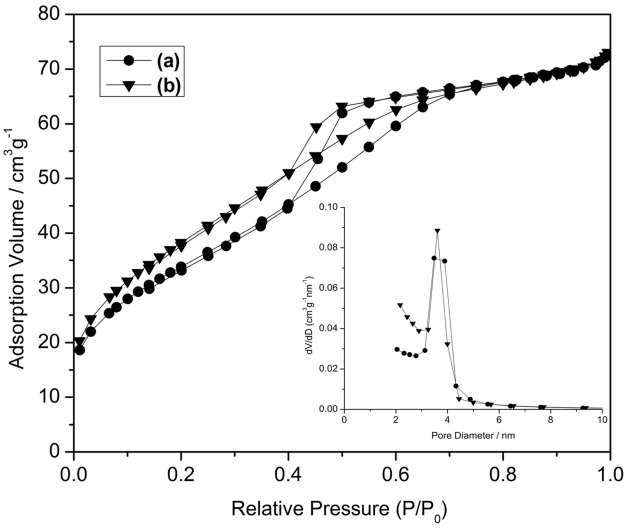

Fig. 8 N_2 adsorption-desorption isotherms of the samples synthesized at different reaction times: (a) 15 min (without ultrasonic treatment); (b) 45 min (with 30 min ultrasonic treatment). The inset shows the pore size distribution of the corresponding samples.

is caused by the sonochemical process. The plot of the pore size distribution (inset in Fig. 8) was determined by using the Barrett-Joyner-Halenda (BJH) method from the desorption branch of the isotherm. It can be seen from the narrow distribution of pore size that almost all the pores can be attributed to mesoporosity. The average pore diameter before and after ultrasound are 3.5 and 3.4 nm, respectively.

Conclusion

In summary, CTHH-$CaMoO_4$ microstructure with uniform morphology as well as controllable size has been synthesized via a facile ultrasound-assisted template-free route at room temperature. The oriented attachment and Ostwald ripening mechanism are proposed to be accounted for the formation of this novel structure via time-dependent observations. It is the influence of the solvent properties of

ethanol and structure-directing effect of EDTA that play pivotal roles in the fabrication of this unique architecture. This novel architecture possessing high specific surface area, hollow interior, mesoporous structure and low density will show better performance in electro-optical devices, scintillators, photoluminescence, etc. This environmentally friendly technique can be applied to synthesize other metal molybdate and tungstate microstructures with complex morphologies.

Notes and references

*Corresponding author. Tel: +86 22 83955762 Fax: +86 22 83955762
E-mail: wanglimin@tjpu.edu.cn; E-mail: dqingchu@163.com
a College of Environment and Chemical Engineering, Tianjin Polytechnic University, Tianjin 300387, PR China.
b College of Material Science and Engineering, Tianjin Polytechnic University, Tianjin 300387, PR China.
c State Key Laboratory of Hollow-Fiber Membrane Materials and Membrane Processes, Tianjin 300387, PR China.
Supporting Information: the controlled experiments, characterization explanations and Fig. S1 are presented as Electronic Supplementary Information.

1 J. Hu, M. Chen, X. S. Fang and L. M. Wu, *Chem. Soc. Rev.*, 2011, 40, 5472–5491.
2 Y. B. Cao, J. M. Fan, L. Y. Bai, F. L. Yuan and Y. F. Chen, *Cryst. Growth Des.*, 2010, 10, 232–236.
3 P. Podsiadlo, S. G. Kwon, B. Koo, B. Lee, V. B. Prakapenka, P. Dera, K. K. Zhuravlev, G. Krylova and E. V. Shevchenko, *J. Am. Chem. Soc*., 2013, 135, 2435–2438.
4 G. S. R. Raju, E. Pavitra, Y. H. Ko and J. S. Yu, *J. Mater. Chem.*, 2012, 22, 15562–15569.
5 V. B. Mikhailik and H. Kraus, *Phys. Status Solidi B*, 2010, 247, 1583–1599.
6 S. Dutta, S. Som and S. K. Sharma, *Dalton Trans.*, 2013, 42, 9654–9661.
7 A. K. Parchur, A. I. Prasad, A. A. Ansari, S. B. Rai and R. S. Ningthoujam, *Dalton Trans.*, 2012, 41, 11032–11045.
8 B. P. Singh, A. K. Parchur, R. S. Ningthoujam, A. A. Ansari, P. Singh and S. B. Rai, *Dalton Trans.*, 2014, 43, 4779–4789.
9 A. K. Parchur and R. S. Ningthoujam, *Dalton Trans.*, 2011, 40, 7590–7594.
10 L. N. Wang, Y. Sun, C. S. Li, Y. Z. Wang, X. G. Ma, Y. D. Wang, S. S. Li, Z. J. Zhang, P. J. Ma and G. H. Cui, *Cryst. Res. Technol.*, 2012, 47, 1231–1236.
11 Y. G. Liang, X. Y. Han, Z. H. Yi, W. C. Tang, L. Q. Zhou, J. T. Sun, S. J. Yang and Y. H. Zhou, *J. Solid State Electr.*, 2007, 11, 1127–1131.
12 Y. Jin, J. H. Zhang, Z. D. Hao, X. Zhang and X. J. Wang, *J. Alloy Compd.*, 2011, 509, L348–L351.
13 W. S. Wang, L. Zhen, W. Z. Shao and Z. L. Chen, *CrystEngComm*, 2014, 16, 2598–2604.
14 Q. Gong, X. F. Qian, X. D. Ma and Z. K. Zhu, *Cryst. Growth Des.,* 2006, 6, 1821–1825.
15 J. J. Zhang, L. L. Li, W. W. Zi, N. Guo, L. C. Zou, S. C. Gan and G. J. Ji, *J. Phys. Chem. Solids*, 2014, 75, 878–887.
16 Y. Sun, C. S. Li, Z. J. Zhang, X. G. Ma, L. N. Wang, Y. Z. Wang, M. Y. Song, P. J. Ma, L. P. Jiang and Y. M. Guo, *Solid State Sci.*, 2012, 14, 219–224.
17 Y. S. Luo, X. J. Dai, W. D. Zhang, Y. Yang, C. Q. Sun and S. Y. Fu, *Dalton Trans.*, 2010, 39, 2226–2231.
18 G. C. Fan, Z. Y. Huang and T. H. Wang, *Solid State Sci.*, 2013, 16, 121–124.
19 J. Geng, J. J. Zhu and H. Y. Chen, *Cryst. Growth Des.*, 2006, 6,321–326.
20 J. L. Zhang, J. M. Du, B. X. Han, Z. M. Liu, T. Jiang and Z. F. Zhang, *Angew. Chem. Int. Ed.*, 2006, 45, 1116–1119.
21 C. C. Yu, M. Yu, C. X. Li, C. M. Zhang, P. P. Yang and J. Lin, *Cryst. Growth Des.*, 2009, 9,783–791.
22 S. F. Wang, F. Gu and M. K. Lu, *Langmuir*, 2006, 22, 398–401.
23 J. J. Zhu, S. Xu, H. Wang, J. M. Zhu and H. Y. Chen, *Adv. Mater.*, 2003, 15, 156–159
24 N. A. Dhas and K. S. Suslick, *J. Am. Chem. Soc.*, 2005, 127, 2368–2369.
25 X. W. Lou, Y. Wang, C. L. Yuan, J. Y. Lee and L. A. Archer, *Adv. Mater.*, 2006, 18, 2325–2329.
26 Y. J. Xiong, B. Wiley, J. Y. Chen, Z. Y. Li, Y. D. Yin and Y. N. Xia, *Angew. Chem. Int. Ed.*, 2005, 44, 7913–7917.
27 Y. S. Wu, H. Yu, F. Peng and H. J. Wang, *Mater. Lett.*, 2012, 67, 245–247.
28 H. G. Yang and H. C. Zeng, *J. Phys. Chem. B,* 2004, 108, 3492–3495.
29 A. X. Wang, D. Q. Chu, L. M. Wang, B. G. Mao, H. M. Sun and Z. C. Ma, *RSC Adv.*, 2014, 4, 7545–7548.
30 Y. K. Yin, F. H. Yang, Y. Yang, Z. B. Gan, Z. M. Qin, S. Gao, B. B. Zhou and X. X. Li, *Superlattice. Microst.*, 2011, 49, 599–607.
31 H. P. Cong and S. H. Yu, *Cryst. Growth Des.,* 2009, 9, 210–217.
32 T. S. Sreeprasad and T. Pradeep, *Langmuir*, 2011, 27, 3381–3390.
33 Y. K. Yin, Y. Li, H. F. Zhang, F. Y. Ren, D. W. Zhang, W. X. Feng, L. L. Shao, K. J. Li, Y. Liu, Z. P. Sun, M. J. Li, G. C. Song and G. Wang, *Superlattice. Microst.,* 2013, 55, 109–117.
34 Y. K. Yin, Z. B. Gan, Y. Z. Sun, B. B. Zhou, X. Zhang, D. W. Zhang and P. Gao, *Mater. Lett*., 2010, 64, 789–792.
35 H. Deng, C. M. Liu, S. H. Yang, S. Xiao, Z. K. Zhou and Q. Q. Wang, *Cryst. Growth Des.*, 2008, 8, 4432–4439.
36 J. Tang and A. P. Alivisatos, *Nano Lett.*, 2006, 6, 2701–2706.
37 R. L. Penn and J. F. Banfield, *Science*, 1998, 281, 969–971.
38 M. Iafisco, G. B. Ramírez-Rodríguez, Y. Sakhno, A. Tampieri, G. Martra, J. Gómez-Morales and J. M. Delgado-López, *CrystEngComm*, 2015, 17, 507–511.
39 D. S. Li, M. H. Nielsen, J. R. I. Lee, C. Frandsen, J. F. Banfield and J. J. De Yoreo, *Science*, 2012, 336, 1014–1018.
40 L. Zhou, W. Z. Wang, H. L. Xu and S. M. Sun, *Cryst. Growth Des.*, 2008, 8, 3595–3601.
41 G. Z. Chen, C. X. Xu, X. Y. Song, S. L. Xu, Y. Ding and S. X. Sun, *Cryst. Growth Des.*, 2008, 8, 4449–4453.
42 Y. D. Hou, X. C. Wang, L. Wu, Z. X. Ding and X. Z. Fu, *Environ. Sci. Technol.*, 2006, 40, 5799–5803.
43 P. Zarabadi-Poor, A. Badiei, B. D. Fahlman, P. Arab and G. M. Ziarani, *Ind. Eng. Chem. Res.*, 2011, 50, 10036–10040.